# Demonstrations of a Fast 4D TEM System for UXO Characterization


Dr. Donald D. Snyder, III
Zonge Engineering and Research Organization, Inc.
Tucson, AZ
SkipS@Zonge.com
David C. George, Dr. Jennifer Hare, Dr. Scott C. MacInnes, Dr. Kenneth L. Zonge


## Static Mode Interpretation

**Static Data Acquisition**

**Static Point Transient Data**

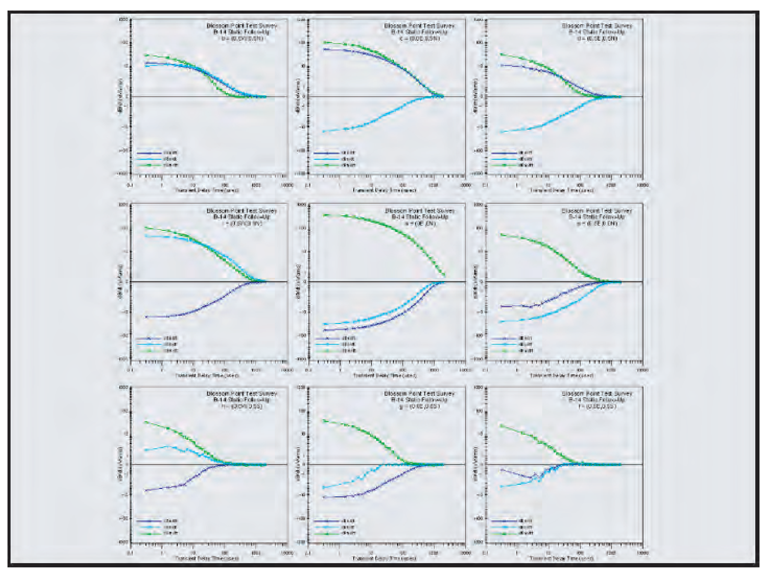

**Inversion Parameters: MK23**

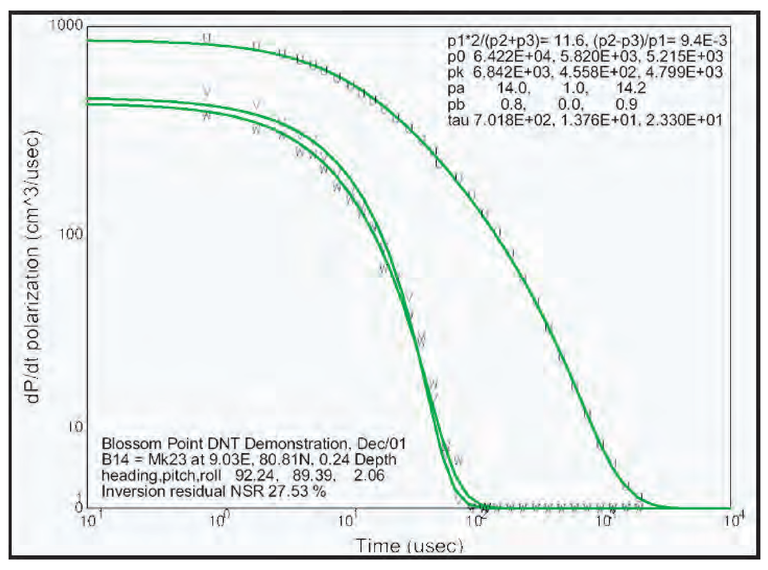


### Static Mode Interpretation

Static mode data are acquired with a static antenna array that is placed at a number of discrete locations (i.e., "9-Spots" at Blossom Point). The antenna position and attitude are carefully controlled and the data at each point have low noise because of our ability to stack many transients and thereby substantially reducing random noise. The nearby panel illustrates a) the field setup, b) the resulting data patch (9x3 transient components), and c) the resulting model-based polarizability plot showing the principal polarizability transients and their parametric representation. This example is for a Mk23 practice bomb (letter 'M' in the photo). The resulting 3 polarizability transients have characteristics typical of a UXO-like object:

1. The largest polarizability is along the axis of symmetry (U-axis)
2. The two minor polarizability transients are similar in shape and magnitude.
3. The slope of the power-law decay parameterization (pk) is greater than 0.7 suggesting a magnetically permeable body.

**Target Items - Blossom Point**


## Dynamic Mode Interpretation

**Dynamic Data Acquisition**

**Dynamic Data (Single Time Gate)**

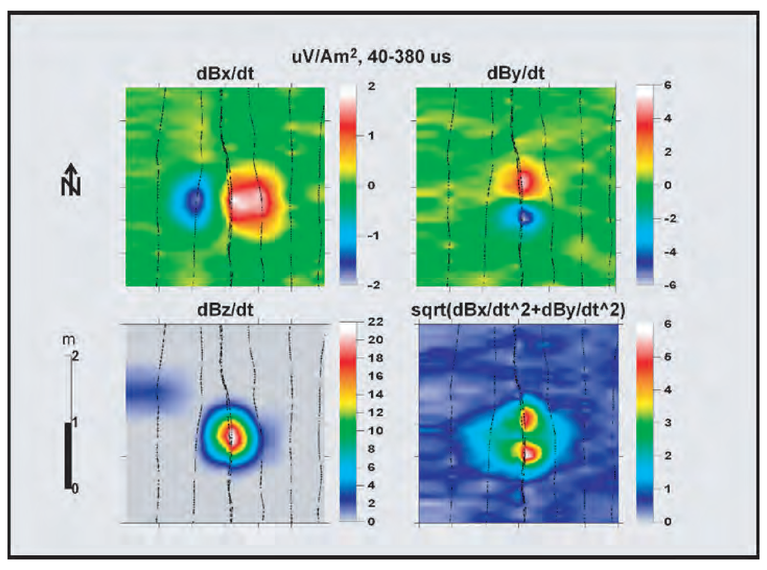


**Inversion Parameters: MK23**

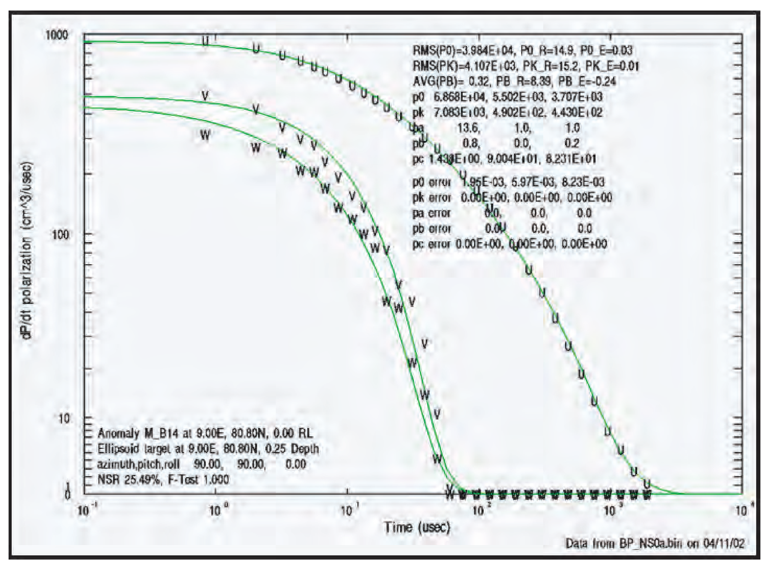


### Dynamic Mode Interpretation

Data acquisition in the dynamic mode is significantly faster. However, because the antenna cart is continuously moving at a rate of 30-60m/min, the quality of the transients at each data point is not as good as that acquired in the static mode. None-the-less, when the signal level is high (as with relatively large and/or shallow targets), the dipole model interpretation methodology produces results that are remarkably consistent with those generated using static data. The figure sequence above again illustrates a) the field setup, b) a data patch showing the 3-component data (mid time composite gate), and c) the resulting model-based decomposition. Note the similarity in the polarizability transients between the statically acquired data and the dynamically acquired data.

## Model-Based Interpretation

### DNT_Dipole (Model-Based Interpretation)

DNT_Dipole fits 3-component transient data in the vicinity of each of a list of targets designated within Oasis Montaj to a point dipole model having an anisotropic polarizability tensor. The geometry and mathematics involved are illustrated below. The model is widely used within the UXO community, providing estimates of the target polarizability along 3 principal axes. These polarizabilities are proportional to the TEM transients that one would measure if the target response were oriented so that its principal axes are in turn parallel with a uniform polarizing magnetic field. DNT_Dipole estimates the 3 principal polarizability transients ($dp_i/dt$; $i = \{u,v,w\}$) using the multi-component transient data acquired by the NanoTEM system. DNT_Dipole also estimates the target position, and attitude angles ($\varphi$=heading, $\theta$=pitch, and $\delta$=roll).

The figures above illustrate DNT data flow from acquisition (LEFT), to processed local data patch (CENTER), and finally to the interpretation parameters (RIGHT). The figure sequences illustrate static acquisition (UPPER) and dynamic acquisition (LOWER). For the MK23 target at Blossom Point, both acquisition methods yield remarkably similar results.

### Implications for Discrimination

Parameters derived from modeling helps to differentiate target types. The "3-β's" introduced by Barrow and Nelson (2001) are similar to the three values of P0 that we calculate for each model using DNT_Dipole. However, our *Polarizability* plot varies slightly from that of Barrow and Nelson. Our plotting method is illustrated in the figure on the right.

* **Rod-like Targets** $P0_U > P0_V \approx P0_W$ and $(P0_V - P0_W) >> (P0_U - P0_V)$: we plot the point $(P0_U, \sqrt{P0_V P0_W})$. We plot the spread of the minor polarizabilities (i.e., $P0_V, P0_W$) as a vertical line through the point.
* **Plate-like Targets** $P0_U \approx P0_V > P0_W$ and $(P0_V - P0_W) << (P0_U - P0_V)$: we plot the point $(\sqrt{P0_U P0_V}, P0_W)$. We plot the spread of the major polarizabilities (i.e., $P0_U, P0_V$) as a horizontal line through the point.
* **Symmetry**: In the Polarizability plot, symmetry is indicated by the length of the vertical/horizontal line. Short lines indicate good symmetry. Long lines mean little or no symmetry.

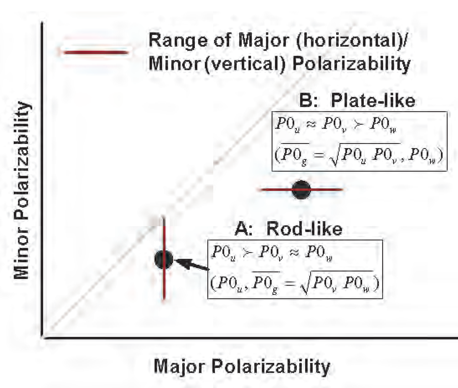


### Polarizability Plots - Blossom Point Targets

The six Polarizability plots below summarize one way in which the model-based parameterization helps to differentiate targets:

a) **All Targets** - We plot polarizabilities for 67 targets at Blossom Point as undifferentiated points.

b) **Cylinder Targets** - We plot only the cylinder targets. Although a few of the targets suggest a plate-like behavior (horizontal lines), all targets exhibit excellent symmetry (short lines). Furthermore, when further differentiated, the points show a distinct relationship between target size and volume.

c) **60mm Mortars** - The target points cluster well and exhibit excellent rod-like characteristics.

d) **Clutter Targets** - The clutter targets fall into two classes. Those with little symmetry (i.e., long lines) and those with good plate-like or rod-like symmetry (short lines). The latter targets are all from "box fins".

e) **Square Plate Targets** - The equi-dimensional steel plate targets show excellent plate-like symmetry (short horizontal lines).

f) **Rectangular Plate Targets** - Rectangular plates exhibit rod-like characteristics. However, their symmetry characteristics are not as good as the cylinders.

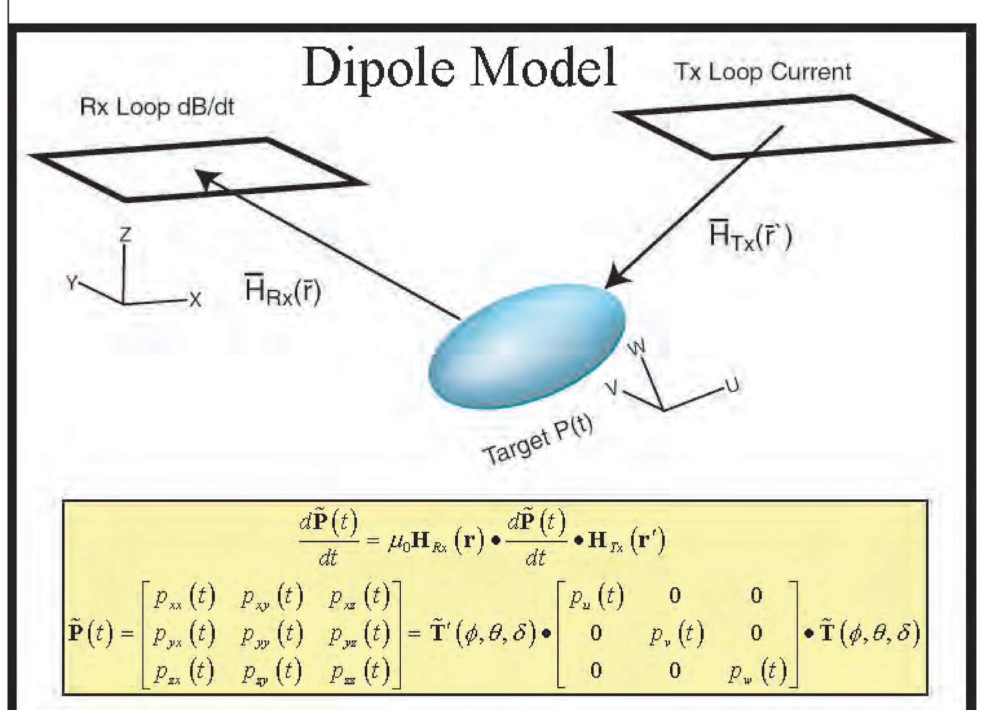


$$\frac{d\bar{\mathbf{P}}(t)}{dt} = \mu_0 \mathbf{H}_{Rx}(\mathbf{r}) \bullet \frac{d\bar{\mathbf{P}}(t)}{dt} \bullet \mathbf{H}_{Tx}(\mathbf{r}')$$

$$\bar{\mathbf{P}}(t) = \begin{bmatrix} p_{xx}(t) & p_{xy}(t) & p_{xz}(t) \\ p_{yx}(t) & p_{yy}(t) & p_{yz}(t) \\ p_{zx}(t) & p_{zy}(t) & p_{zz}(t) \end{bmatrix} = \bar{\mathbf{T}}'(\phi,\theta,\delta) \bullet \begin{bmatrix} p_u(t) & 0 & 0 \\ 0 & p_v(t) & 0 \\ 0 & 0 & p_w(t) \end{bmatrix} \bullet \bar{\mathbf{T}}(\phi,\theta,\delta)$$

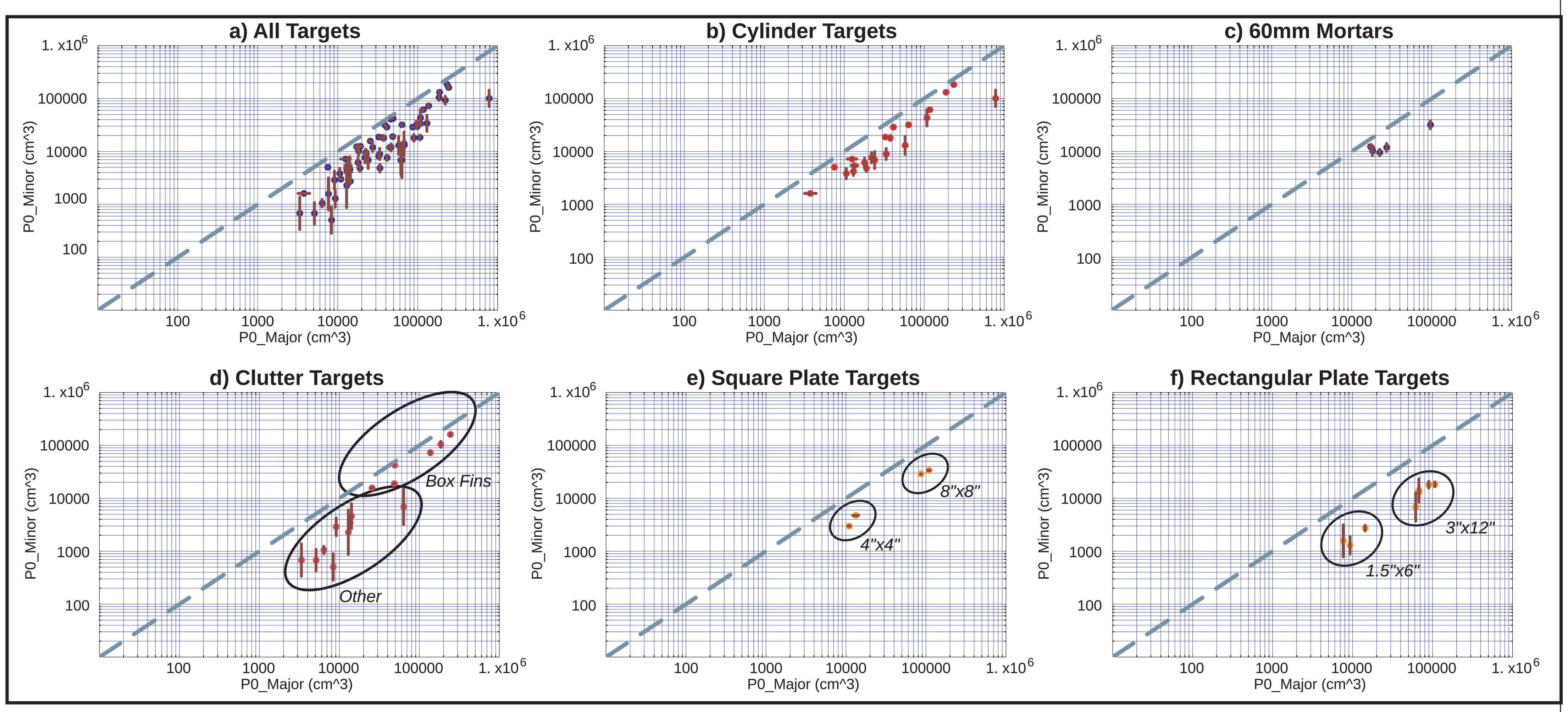


## 1999 Continuous NanoTEM Developed

In 1999, Zonge modified the NanoTEM acquisition program to permit continuous acquisition of NanoTEM data. Although then limited to a sample rate of 1Hz, Continuous NanoTEM has been used successfully on several UXO projects (e.g., Gambell, Alaska, shown below, and Waikoloa, Hawaii) and on numerous environmental projects. Development began on a new program, "DynanoTEM", or DNT, that permitted multi-channel data acquisition at sample rates as high as 32 Hz.

**2000 Continued Antenna Development and ESTCP Award**

In 2000, Zonge continued internally-funded work to develop the NanoTEM system for UXO detection and characterization. We constructed a 2nd generation antenna cart and tested it both in moving and static modes. We submitted a proposal to ESTCP titled “UXO Characterization With a Fast 4-D TEM System”. We were awarded a contract (ESTCP No. 200105) and work commenced in May, 2001.